Chemical Engineering Journal 412 (2021) 128647

Contents lists available at ScienceDirect

Chemical Engineering Journal

journal homepage: www.elsevier.com/locate/cej

Thermal stable honokiol-derived epoxy resin with reinforced thermal conductivity, dielectric properties and flame resistance

Jingjing Meng [a,1], Pengfei Chen [a,1], Rui Yang [a], Linli Dai [a], Cheng Yao [b], Zheng Fang [a], Kai Guo [a,*]

[a] College of Biotechnology and Pharmaceutical Engineering, Nanjing Tech University, Nanjing 211816, PR China
[b] College of Chemistry and Molecular Engineering, Nanjing Tech University, Nanjing 211816, PR China

ARTICLE INFO

Keywords:
Honokiol
Epoxy resin
Thermal stability
Thermal conductivity
Dielectric constant
Flame retardancy

ABSTRACT

To produce renewable and functional epoxy resins, novel polymers were fabricated based on naturally available honokiol. The honokiol-derived (DBDBBB) epoxy resin monomer was firstly reported and cured by diamino diphenyl-sulfone (33DDS and 44DDS). The resultant networks were fabricated via both epoxy resin and polyolefin, and showed excellent thermal stability (T_{max} up to 451 °C), thermal conductivity (~0.743 W/m•K), and high specific heat (5.364 J/g•K) as well as the excellent dielectric constant and loss values (9.74, 0.026) (1 kHz, 25 °C). Moreover, the bio-based networks were low flammable. The high-performing DBDBBB/DDS networks surpass the DGEBA analogs, and hence it will be a promising candidate for DGEBA and has great potential application in the electronics and microelectronics industry.

1. Introduction

With the development of chemicals, wanton depletion of oil reserves occurs. Regardless of the great progress in the past decades, several serious problems concerning the ecological environment deterioration in some regions, atmosphere pollution, and even the industrial air pollution situation have aroused widespread concern. It is worth emphasizing that, especially, due to the increasing industrial growth, the petrochemical feedstocks are getting tense. In the long term, the establishment of bioconversion procedures for biomass products is not only promising but also inevitable for substituting the petrochemicals. The progressive elimination of the routes with high consumption of energy, heavy pollution, and low technology makes this alternative protocol more meaningful. These related technical development and promotion are strikingly bloomed in several aspects, such as fuels, fine chemicals, and polymers even on a large scale [1–4].

As we know, epoxy resins are predominately synthesized from non-renewable resources heretofore. Typically, diglycidyl ether of bisphenol A (DGEBA) synthesis heavily relies on nonrenewable bisphenol A (BPA). However, the BPA is derived from petroleum-based phenol and acetone [5], which reacts with environment-friendly epichlorohydrin (ECH) via an O-glycidylation reaction affording DGEBA [6]. Currently, >90% of the commercial epoxy resins are fabricated from DGEBA. Although those DGEBA epoxy resin networks have high glass transition temperatures and good thermal stability, several disadvantages resulted from BPA, such as carcinogenicity, mutagenicity, and reprotoxicity as well as endocrine disruptors, have given rise to the public attention for its substitution [7]. Thus the BPA-containing items are highly restricted to baby collections and medical supplies. Over the past decades, alternatively, many attempts have been made to find promising renewable stocks.

An increasing amount of feedstocks transformed from plants and herbs via extraction and fermentation offer a promising perspective for the development of novel bio-based polymers. It was considered as a versatile but cost-effective strategy for biomass materials with diverse functions. Most impressively, up to date, various biomasses, for instance, resveratrol [8], magnolol [9], daidzein [10], eugenol [11,12], quercetin [13], and protocatechualdehyde [14] are introduced into epoxy resin polymers exerting them with several superior performances, such as excellent thermal stability, flame retardancy, and thermal conductivity as well as electrical performance. Mostly, those bio-based aromatic compounds behave good mechanical properties, and partially some fascinating merits confer the corresponding functional features to bio-based epoxy networks. Albeit a few linear and hyperbranched epoxy-ended monomers based on petroleum chemicals can also endow polymers with several comparative advantages [15].

* Corresponding author.
E-mail address: guok@njtech.edu.cn (K. Guo).
[1] These authors contributed equally to this work.

https://doi.org/10.1016/j.cej.2021.128647
Received 13 September 2020; Received in revised form 20 December 2020; Accepted 18 January 2021
Available online 23 January 2021

The past decades witness the rapid growth of bio-epoxy resins and further indicate their great superiorities over the petro-based analogs. However, a great challenge remains as to the net thermosets with high thermal, mechanical properties and conductivity as well as flame resistance. Recently, the carbon nanotube is mainly reported to update the electrical conductivity of the epoxy composites [16]. Beyond this, various attractive protocols, for instance, the high-order composites with mesogen segments or the bottom-up parallel-linking and strain strategy has been disclosed and greatly elevates the thermal conductivity of bulk epoxy resin (>0.96 W/m·K) [17,18]. To enhance the thermal conductivity, different fillers such as natural graphite and graphene are adulterated into the epoxy resin system [19,20]. Except for those points, various components are solely employed to raise the flame-retardant efficiency in epoxy resins. For example, black phosphorene [21,22] and carbon fiber [23], carboranes [24] are commonly introduced. Moreover, several other fillers containing the following elements, such as organic phosphorus [25], borates [26,27], and silicon [28], so on [29–31], can remarkably augment the fire resistance. Despite those excellent performances, those works relied heavily on crude petroleum but lacked in sustainability and development.

Herein, a novel bio-based honokiol, namely 2,2′-(((3′,5-diallyl-[1,1′-biphenyl]-2,4′-diyl)bis (oxy))bis(methylene)) bis(oxirane) (DBDBBB) was synthesized, and introduced into the thermosetting epoxy resins. The concerning issues were thoroughly investigated, and the results proved that DBDBBB/DDS matrixes exhibited excellent properties. For instance, DBDBBB/44DDS showed the highest thermal stability among bio-based epoxy resins reported to date. Besides that, it also possessed excellent dielectric constant and loss values, as well as good thermal diffusivity and conductivity. Meanwhile, its DBDBBB/33DDS analog also showed superior performance of lap shear strength, specific heat, and flame resistance. Accordingly, these comprehensive properties of bio-epoxy resin polymeric networks will successfully arouse its potential application in fire protective coatings, electronics and capacitors, etc.

2. Materials and methods

2.1. Materials

Honokiol (98% purity), tetrabutylammonium bromide (TBAB, 98% purity), bisphenol A diglycidyl ether (DGEBA, >85%), 3,3′-diamino diphenyl-sulfone (33DDS, >99% purity) and 4,4′-diamino diphenyl-sulfone (44DDS, >99% purity) were obtained from Macklin Reagent Company, China. Sodium hydroxide (NaOH) and epichlorohydrin (ECH, 99%) were from Aladdin Chemical Reagent, China.

2.2. Honokiol-based epoxy monomer (DBDBBB) synthesis

The epichlorohydrin (0.7 mol, 64.75 g) and tetrabutylammonium bromide (5 mmol, 1.61 g) were added in 50 wt% aqueous solution NaOH (24 g NaOH /24 g H_2O), and then the mixture was agitated vigorously at room temperature for 0.5 h. Afterward, the solution of honokiol (50 mmol, 13.31 g) in THF (60 mL) was added dropwise under N_2 flow. Upon completion, the reaction occurred at 50 °C until TLC (PE/EA = 4/1) indicated the complete consumption of honokiol. Methylene chloride was directly used to extract the product three times. The obtained organic phase was washed with water and brine, which finally dried over Na_2SO_4. Subsequently, the filtration and evaporation allowed the samples for separation through silica gel column chromatography with gradient elution (PE/EA, 30/1 to 6/1). The transparent, colorless adhesive liquid DBDBBB (15.4 g) was in 81.5% yield. The synthetic route for DBDBBB is presented in Fig. 1.

2.3. General procedure for the honokiol-based epoxy resin matrixes

To produce biomass-based epoxy resin with excellent performance, the epoxy resin DBDBBB/DDS was prepared via a curing process of DBDBBB with DDS (with the molar ration of an epoxy group to NH in 1:1). The stoichiometric blends of DBDBBB and DDS were mixed homogeneously at room temperature under N_2, and then warmed up in the respective liquefied temperature range. With the temperature increasing, a resultant colorless melted mixture with low viscosity formed. The mixture was poured into the preheated stainless steel mould (170 °C). Remarkably, little mold spray should be smeared on the mould surface before injection. Then the injected steel mould was heated to a given curing temperature in 1 h. Next, the curing process occurred at 210 or 215 °C for about 2 h. The mould was then naturally cooled and ready for a demoulding process. The procedure concerning DGEBA/DDS matrixes followed the analogous process. All newly manufactured epoxy resins were kept for two weeks before determinations. The formulations of DBDBBB/DDS and DGEBA/DDS are displayed in Table 1.

2.4. Measurement and characterization

2.4.1. FTIR

Fourier transform infrared (FTIR) determination was performed on a Bruker a Vertex 70 spectrometer (USA) over the wavenumber ranging from 400 to 4000 cm^{-1}. All samples were scanned for 16 times.

2.4.2. NMR

The characterization for both monomers and chemical structure of polymers was performed on Bruker ADVANCED III (400 MHz) spectrometers for the NMR test. $CDCl_3$ was employed for dissolving the samples.

2.4.3. HRMS

High-resolution mass spectra (HRMS) were performed on Agilent mass spectrometer with ESI-TOF (electrospray ionization-time of flight).

Table 1
The formulations of DBDBBB/DDS and DGEBA/DDS.

Samples	DBDBBB (g)	DGEBA (g)	DDS (g)	Liquefied temp. range (°C)	Curing temp. (°C)
DBDBBB/33DDS	7.56	–	2.48	130–195	210
DBDBBB/44DDS	7.56	–	2.48	130–185	210
DGEBA/33DDS	–	6.81	2.48	165–195	215
DGEBA/44DDS	–	6.81	2.48	165–195	215

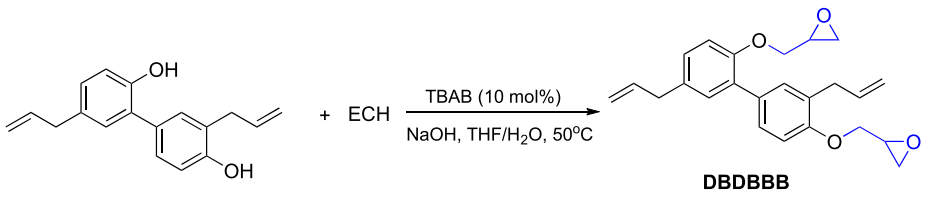

Fig. 1. One-pot synthesis of DBDBBB.

2.4.4. TG

Thermogravimetric analyzer (TGA) and differential thermogravimetry (DTG) ranging from 40 to 900 °C were performed on a Discovery TGA-550 system under a nitrogen flow of 20 mL/min and a heating rate of 20 °C/min. NETZSCH TG 209F1 Libra was employed for the TG test in an atmosphere of 20% oxygen and 80% nitrogen.

2.4.5. DMA

Dynamic thermomechanical analyzer (DMA, US) was performed on Diamond DMA under a single cantilever bending mode at a frequency of 1 Hz. Each sample was scanned from 0 to 300 °C at a heating rate of 3 °C/min. The dimensions of the specimen were 10 mm*5 mm*3 mm.

2.4.6. Mechanical test

Flexural strengths and moduli were measured according to GB T 9341-2008/ISO 178:2001 at a speed of 2 mm/min on an electronic universal testing machine (Shenzhen SUNS Technology Stock Co. LTD, China). Shore hardness (D) values were achieved following ASTM D2240 on Shore Hardness Tester (HT-6510D). Lap Shear Strength of bonding samples was measured at room temperature according to the Chinese standard GB7124-86 at a speed of 5 mm/min and the shear strength (τ) is calculated as $\tau = N_{max}/S$, where N_{max} is the maximum tensile force and S is the overlap area. Adhesion tests were performed on PosiTest AT-M with tapered pins (20 mm head diameter) according to ASTM D4541.

2.4.7. SEM

Microscopy analysis was performed on the scanning electron microscope (SEM TM3000, Hitachi, the largest magnification up to 10000). The sample was sputter-coated with gold before testing.

2.4.8. Dielectric properties

Dielectric properties were measured on a broadband dielectrics spectrometer (Novocontrol Concept 80, Hundsangen, Germany) at room temperature over the frequency from 0 to 3 MHz. The diameter of each sample was 10 mm with a thickness 3 mm on round plate electrode.

2.4.9. Thermal conductivity

The thermal diffusion coefficient was carried out on the NETZSCH LFA 427 with a laser flash analysis. The disk with a diameter in 12.7 mm and 2 mm in thickness was determined at 25 °C.

The epoxy resin disks with a diameter of 12.7 mm and 1 mm in thickness were used for thermal conductivity estimation. The thermal transmission process was recorded on an infrared thermal imager (Testo 875i). The heater was heated to a fixed preset temperature (150 °C). Once the disk was placed on the heating plate, its surface temperature was recorded with a 5 s time interval.

2.4.10. Horizontal burning test

The horizontal burning procedure was conducted using the cured epoxy resins. The specimens (thickness 3 mm and width 20 mm) was horizontally located, and the front of the samples was ignited about 10 s.

2.4.11. MCC

In the microscale combustion calorimetry (MCC-2, Govmark) experiments, about 5 mg sample was heated to 900 °C with a heating rate of 1 °C/s at a stream of nitrogen flowing of 80 cm^3/min. The volatile and anaerobic thermal degradation molecules in the nitrogen stream were mixed with a 20 cm^3/min stream comprised of 20% oxygen and 80% nitrogen before approaching a combustion furnace at 900 °C.

3. Results and discussion

3.1. Synthesis and characterization of DBDBBB

The chemical structures of DBDBBB and honokiol were characterized by the NMR (Fig. 2 and Fig. S1), IR (Fig. S2), and HRMS (Fig. S3). It was disclosed that the characteristic peaks of phenolic OH in the honokiol at about 5.25 ppm, and it disappeared once the O-glycidylation reaction occurred. The resultant peaks at about 3.9 ~ 4.3, 3.2 ~ 3.4, and 2.6 ~ 2.9 ppm corresponded to the epoxy motifs. Furthermore, it was confirmed that the ^{13}C NMR spectra that 69.08, 68.75, 50.27, 50.21, 44.57, 44.55 peaks were attributed to carbons on epoxy groups in DBDBBB. The comparison between DBDBBB and honokiol suggested the full etherification of phenolic OH, and thus afforded the novel bio-epoxy resin monomer, as a colorless sticky liquid.

3.2. Heat curing behaviors of epoxy resins

To estimate the curing process, the traditional IR technique was employed. The distribution of oxirane and NH_2 residue in the matrix were directly used to monitor the reaction process (Fig. S4 and Fig. 3). In Fig. S4, the spectra of monomers, such as DGEBA, DBDBBB, and 33DDS as well as 44DDS were presented. The absorption located about 900–680, 1500, and 1600 cm^{-1} were generated from the C=C stretching and C–H deformation on the aromatic rings. As to DDS hardeners, the representative absorption peaks for active NH_2 functionality were located at around 1623, 3330, 3360, and 3380 cm^{-1}. Such peaks were employed as references for independently monitoring the reaction. It was obvious that, in terms of the DDS, the absorption at about 1630 cm^{-1} vanished completely indicating the full polymerization.

The oxirane motifs represented three typical peaks at about 850, 910, and 1240 cm^{-1} due to the asymmetric and symmetric bending vibrations of C–H [32]. Alternatively, the peak at 910 cm^{-1} was often used to estimate the reaction process. It was evident that, for DGEBA/DDS networks, both absorptions at 850 and 910 cm^{-1} disappeared (Fig. S4b). However, for DBDBBB/DDS, the separate peak at 850 cm^{-1} significantly faded, while the bending vibration of terminal CH = CH_2 at 912 cm^{-1} was confusingly similar to that of waned oxirane (about 910 cm^{-1}). Therefore, both the peaks of reactive oxirane (about 850, 912 cm^{-1}) and NH_2 (around 1623 cm^{-1}) were taken to monitor the polymerization process [32]. As depicted in Fig. 3, in the fully cured epoxy resin fabrications, a wide absorption peak at ~ 3400 cm^{-1} formed as a result of the ring-opening of oxirane leading to the appearance of the OH group. Moreover, the aliphatic C-N stretching vibration at 1237 cm^{-1} suggested the nucleophilic reaction occurred. Overall, the curves in Fig. 3 suggest the elimination of reactive functions confirming the complete polymerization of epoxy motifs. On the other hand, it was seen that there existed a small amount of allyl functional groups (1640 cm^{-1}) remained for both DBDBBB/33DDS and DBDBBB/44DDS (Fig. S2 and Fig. 3), which indicated the relatively slow polyolefin process. Thus, the DBDBBB/DDS networks were fabricated via both epoxy resin and polyolefin.

3.3. Thermal stability of epoxy resins

The thermal stabilities of DBDBBB/DDS and DGEBA/DDS were investigated by TGA under an N_2 atmosphere. The curves of corresponding TGA and DTG are showed in Fig. 4. It was disclosed that both DBDBBB/DDS and DGEBA/DDS exhibited extremely high thermal stability. The typical parameters serve as common references for their stability, such as T_{d5} (for 5% degradation), T_{d30} (for 30% degradation), T_{max} (for the maximum decomposition rates from DTG curves), and T_{HRI} as well as R_{800} (char residue at 800 °C) are listed in Table 2. Obviously, DBDBBB/DDS gave comparable T_{d5} values in contrast to the DGEBA counterparts. The differential thermogravimetry (DTG) curves suggested that the DBDBBB/33DDS and DBDBBB/44DDS matrixes promptly decomposed at 450 °C and 451 °C, respectively (Fig. 4b). In contrast to the slightly low T_{max} (no>435 °C) of DGEBA and magnolol-based composites [9], DBDBBB/DDS fabrications possessed a wider working temperature range and comparable transparency (Fig. 4c). Several bio-epoxy resins derived from natural resources have been

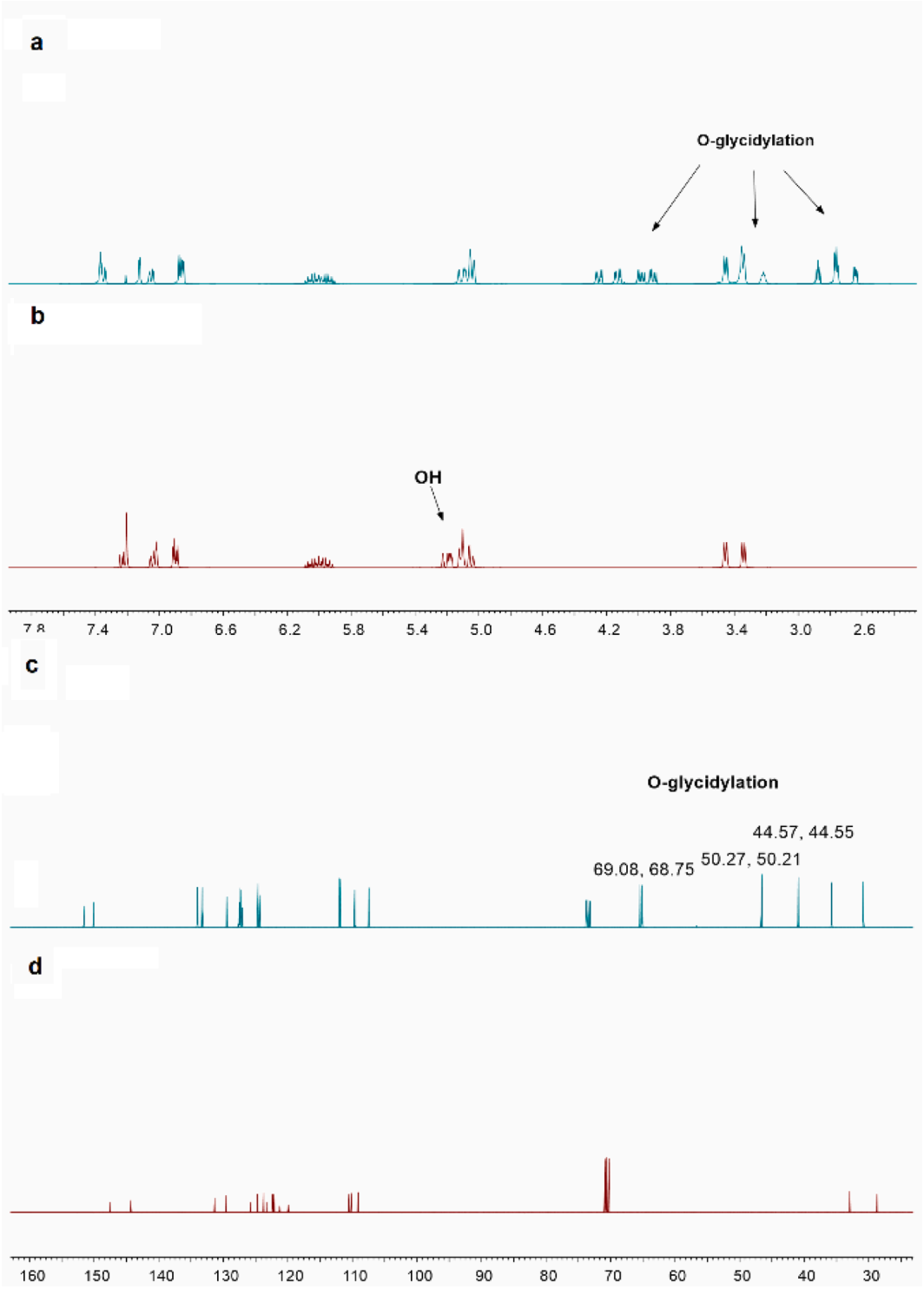

Fig. 2. The NMR spectra of DBDBBB (a, c) and the honokiol (b, d).

summarized in Fig. 4d and Table S1. To date, it has been proved that the novel DBDBBB/44DDS networks presented the highest T_{d5} among the reported bio-based epoxy resins. Notably, DBDBBB/44DDS network also behaved highest heat-resistance index (T_{HRI}) reaching 212.7 °C, indicated its excellent thermal stability [33]. Moreover, it is remarkably impressive that the char residues at about 800 °C for DBDBBB/DDS surpassed that of the DGEBA polymer matrixes. The drastic decomposition in a narrow temperature range (380–390 °C, char residues about 24%) [21] possibly accounted for the highest char residue of the DBDBBB/44DDS network, and this property perhaps denoted its advantageous fire retardancy.

To further confirm the thermal stabilities of those networks, TGA was conducted in air as well. The concerning results are presented in Table S2, and the decomposition behaviors are described in Fig. S5. For DGEBA/DDS, the network was more unstable and could be readily broken down in air in contrast to that in N_2. Conversely, DBDBBB/DDS showed negligible changes in T_{d5}, T_{d30}, and T_{max} either in N_2 or air atmosphere. Apart from this, it was observed that Fig. 4b suggested a one-

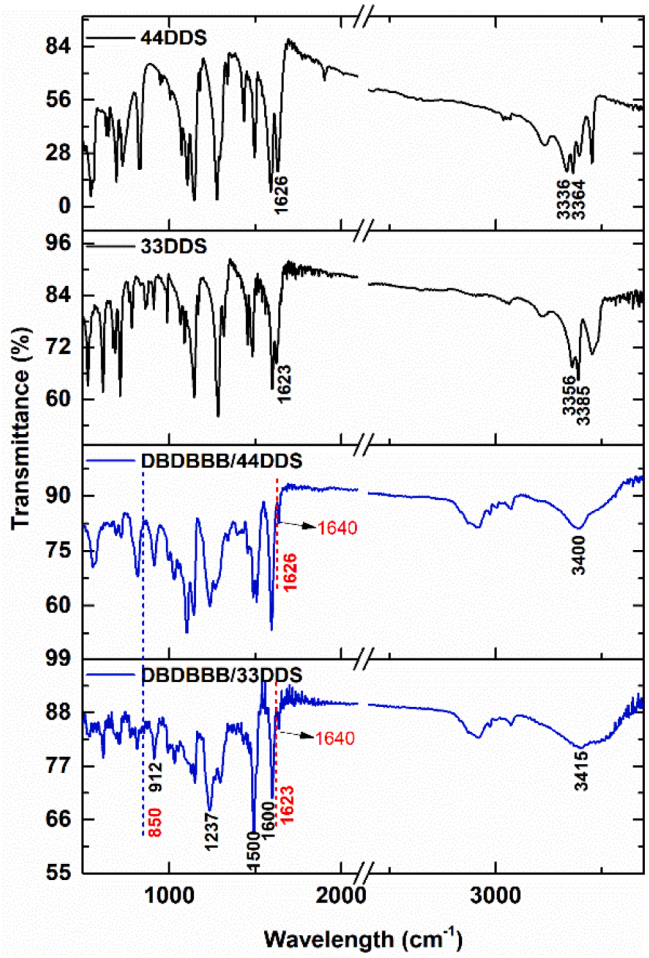

Fig. 3. IR spectra for DDS and DBDBBB/DDS networks.

step pyrolysis in N_2 with a single peak from 320 to 580 °C. In comparison with Fig. 4b, a two-step decomposition occurred with two peaks ranging from 320 to 530 °C and 580 to 760 °C, respectively (Fig. S5b). The thermal decomposition certainly occurred ranging from 320 to 580 °C. Nonetheless, when it happened in air, the free radical polymerization readily formed in-situ and led to more stable polymeric networks with decomposition peaks at about 600 °C. The TG curves in Fig. S5a denotes the char residues for DBDBBB/DDS is higher than DGEBA/DDS. The char residues at both 440 °C and 620 °C were listed in Table S2. For instance, DBDBBB/33DDS showed the highest char residue about 25% at 620 °C, surpassing that of DGEBA/33DDS (15.7%) (Entry 1 *vs* 3, Table S2). It was possibly attributed to the biphenyl motifs in DBDBBB, which promoted a highly thermally resistant carbonaceous during the thermal pyrolysis [9,34]. As a result, the DBDBBB/33DDS exhibited an enhanced fire retardancy in air.

3.4. Dynamic thermomechanical analysis of epoxy resins

The dynamic thermomechanical analyzer (DMA) was employed to investigate the thermomechanical properties involving glass transition temperature, storage modulus, and loss modulus, etc. (Fig. 5). Fig. 5a showed that DBDBBB networks behaved higher storage modulus than DGEBA matrixes before around 100 °C. Afterward, the storage modulus dramatically decreased in the transition region. The DBDBBB/33DDS and DBDBBB/44DDS have the extrapolated *E'* onset temperatures at about 81.3 and 85.1 °C, respectively, which are about 50 °C lower than the DGEBA analogs. Fig. 5b indicates the amorphous DBDBBB networks presenting glass transition temperature (T_g) at 116.1 and 125.3 °C, while DGEBA showing superior T_g values (163.3 and 164.2 °C). It was clearly verified that the symmetric 44DDS endowed the polymer with a higher T_g than the 33DDS did. Such a difference is possibly dependent on the symmetric structure and high crosslinking density. Although it was observed that 33DDS behaved more reactive than 44DDS in the curing process [35], the relatively sluggish 44DDS reacted with the remained epoxy groups finally afforded an aligned structure with higher T_g covering a wider peak width (Fig. 5b). Moreover, it also indicated a relatively long distribution of crosslinking chains [14].

The multiple relaxations properties of amorphous epoxy resins, in general, appeared when the temperature varied. The T_g is mainly determined by the polymer fabrication and segmental restriction of the motion, while the secondary relaxations are driven by the anchored linear chain in the polymeric networks. It was firstly disclosed that, in contrast to the sample cooling at room temperature, the networks annealed respectively at −30 °C and −196 °C, could remarkedly increase the storage moduli. For instance, when DBDBBB/33DDS was annealed at −196 °C, the *E'* increased by 31% (Fig. 5c). Therefore, variation in annealing temperature was proved to be a useful strategy for storage modulus improvement. The secondary relaxations involving the soft segments of polyolefin might be responsible for the low-temperature shoulder in the tan δ-temperature curves, albeit the analogous conformational fluctuations and phenyl ring flipping that cannot be ruled out [35,36]. As shown in Fig. 5d, DBDBBB/44DDS resin displayed a shoulder comparing to 33DDS analog. Furthermore, for 33DDS networks, when the annealing temperature declined, there appeared an identifiable shoulder. Theoretically, those differences were possibly attributed to the variation of the polyolefin motifs shifting to a reasonably free segment while the heating during the DMA determination happened.

Fig. 5e and f illustrate the morphologies of the fracture surface of DBDBBB/DDS. It was visible that DBDBBB/33DDS yielded an interlaced network, wherein the chains twisted widely on the fracture surface, while for DBDBBB/44DDS, a relatively smooth surface occurred with distinct gaps or gullies between the dendritic structures. This indicated the more brittle nature of DBDBBB/44DDS, and an increasing force for propagation might be required for the DBDBBB/33DDS abruption [14].

To elaborate the effect of annealing temperature on DBDBBB/DDS networks, crosslink density (v_e) is calculated for the rubbery elasticity, wherein *E'* signifies the storage modulus at ($T_{g,DMA}$ + 30) °C in the rubbery plateau region, and *T* ($T_{g,DMA}$ + 30) (K) implies the absolute temperature. The *R* denoted gas constant, 8.314 J/ mol•K.

$$v_e = E'/(3RT)$$

As listed in Table 3, with the annealing temperature decreasing, the DBDBBB/DDS networks tend to display higher storage modulus values and increasing crosslinking densities. Especially, when the samples were annealed at −196 °C, the storage modulus and v_e values were remarkably increased (21.5 MPa and 2.070 mol/dm^3, respectively) for the DBDBBB/33DDS. Generally, it was first revealed that 33DDS favored an enhancement in crosslinking densities than 44DDS, and the symmetric linear structure of 44DDS soundly interpreted the main factors in determining the T_g values regardless of varied annealing temperature (entries 1/3/5 *vs* 2/4/6, Table 3). Also, the results further confirmed that in the tan δ-temperature curves, a low tan δ indicated the more intense crosslinking in the networks (Fig. 5d).

3.5. The flexural properties of epoxy networks

The concerning flexural properties and hardness values are also listed in Table 4. The load–deflection features of the bio-based DBDBBB/DDS are described in Fig. 6. The results indicated that the novel DBDBBB/DDS showed moderate flexural strengths. The compromising mechanical properties seem due to the enhanced amorphous structure aroused by non-crystalline DBDBBB [20].Obviously, the curves in Fig. 6 denoted DBDBBB/DDS behaved a brittle nature, and no yielding

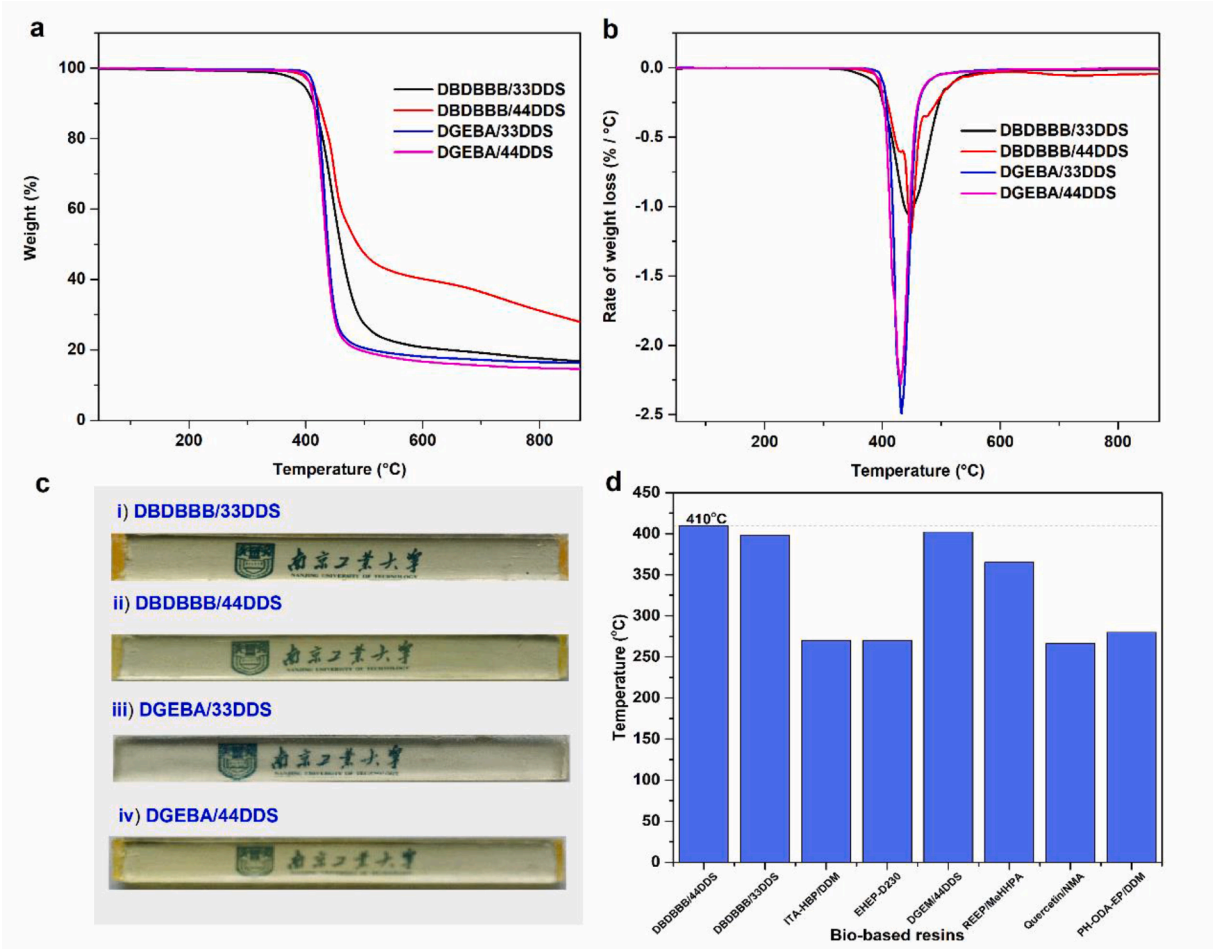

Fig. 4. The degradation curves (a, b) and transparent profiles for DBDBBB/DDS and DGEBA/DDS (c); Representative T_{d5} values for several novel bio-epoxy resins (d).

Table 2
Thermal stabilities of DBDBBB/DDS and DGEBA/DDS.

Entry	Sample	T_{d5} (°C)	T_{d30} (°C)	T_{max} (°C)	T_{HRI} (°C)	R_{800} (%)
1	DBDBBB/33DDS	397	440	450	207.2	17.6
2	DBDBBB/44DDS	410	450	451	212.7	31.2
3	DGEBA/33DDS	413	430	430	207.4	16.5
4	DGEBA/44DDS	408	426	424	205.2	14.8

$T_{Heat\text{-}resistance\ index}(T_{HRI})$ is calculated by following equation: $T_{HRI} = 0.49*[T_{d5} + 0.6*(T_{d30}\text{-}T_{d5})]$.

occurred when the bending proceeded. This was possibly attributed to the rigid diphenyl scaffold in the chains. Furthermore, the lower deflection value suggested the DBDBBB/DDS were more fragile than DGEBA/DDS networks regardless of the comparable modulus. The 33DDS-derived polymers displayed significantly better flexural properties than that of 44DDS. Besides, owing to the increasing chain ductility of polyolefin segments, the DBDBBB/DDS also gave slightly low hardness relative to DGEBA/DDS.

3.6. Lap shear strength of epoxy networks

The lap shear test of the epoxy composite-steel system was undertaken to estimate the bonding strength (Fig. 7a). Regarding DGEBA epoxy resins, 44DDS behaved with slightly better lap shear strength than 33DDS (20.22 > 18.17 MPa). Conversely, for DBDBBB, its 33DDS and 44DDS-derived resins exhibited the values of 24.06 MPa and 13.75 MPa, respectively. Moreover, the morphologies of the fracture surface for each sample facilitated the interpretation the lap shear strength results (Fig. 7b). Because the hydroxyl formation in bulk occurred in the polymerization process, the epoxy resin adhesive significantly enriched the wettability towards the steel surface, and thereby enhanced bonding strength greatly. Indeed, in terms of DBDBBB/33DDS, the cracks were primarily interlaced with each other, therefore leading to a high lap shear strength. Meanwhile, for DGEBA polymers, the crack texture indicated the collapse resulted from the forces working in the opposite direction, wherein crack deflection occurred when tension deformation increased. Besides, as to the DBDBBB/44DDS, bubbles mainly deteriorated the epoxy resin to the steel surface, and thus lowered their lap-shear strength [37,38].

3.7. Adhesion strength of epoxy networks

The adhesion strengths of those epoxy resins are shown in Fig. 8. It was obvious that 33DDS endowed both DGEBA and DBDBBB with lower values than 44DDS, indicating a decreasing bond strength when the tension occurred vertically. In particular, for DBDBBB/44DDS, the adhesion increased significantly relative to DGEBA/44DDS. The much more reactive 33DDS could hamper the flow of the liquefied epoxy resin prepolymer before full curing. In contrast, the DBDBBB/44DDS networks behaved the highest adhesion strength attributed to good flow performance. It filled the holes and depressions on the surface of the

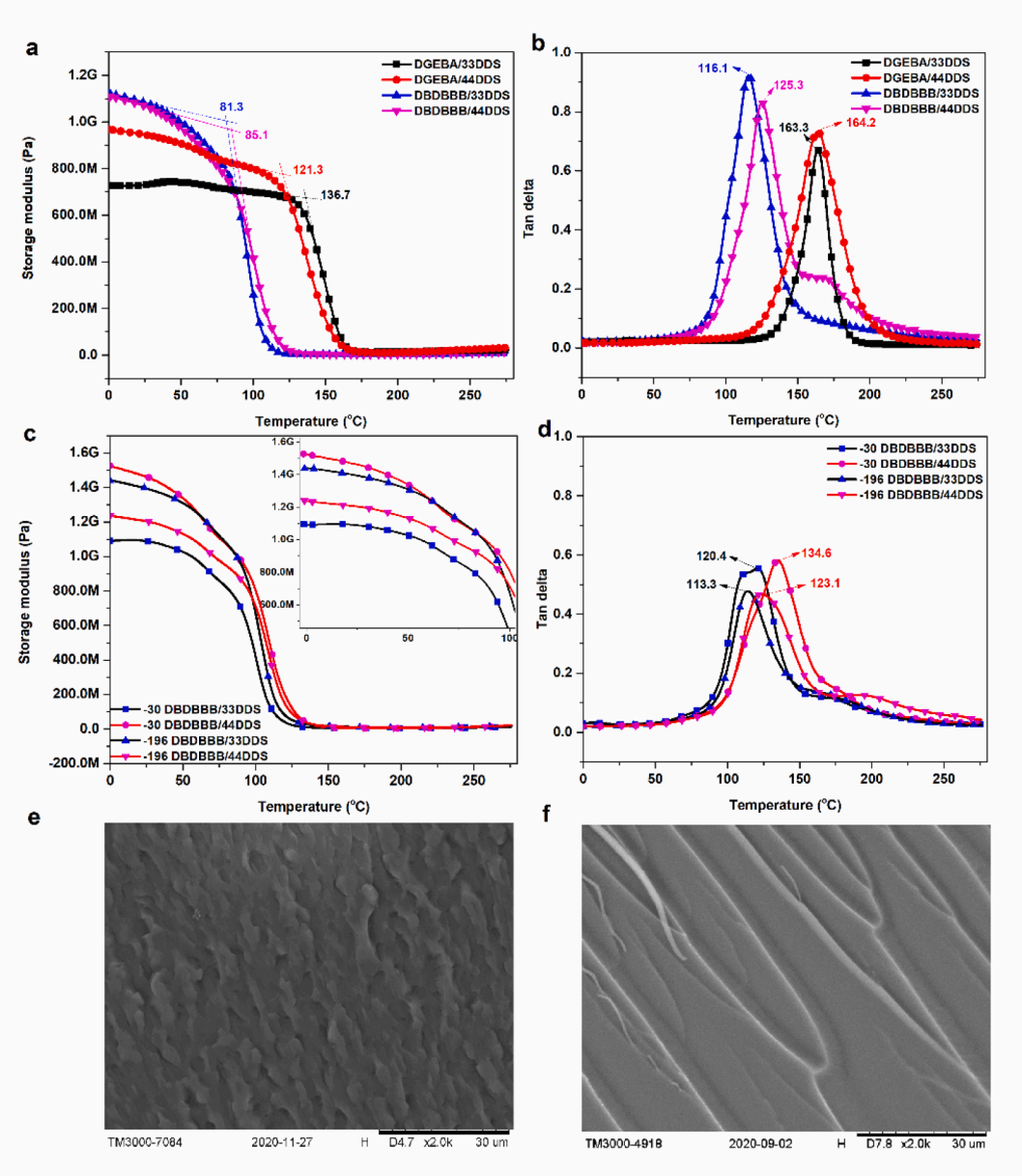

Fig. 5. The DMA profiles of epoxy thermosets annealed at 25, −30 and −196 °C (a/c. storage modulus; b/d. tan δ). The fracture surface of DBDBBB/33DDS (e) and DBDBBB/44DDS (f), respectively.

Table 3
Dynamic mechanical properties.

Entry	Sample	E' (GPa)[c]	E' (MPa)[d]	$T_{g,DMA}$ (°C)	ν_e (mol/dm^3)
1	DBDBBB/33DDS	1.08	1.94	116.1	0.185
2	DBDBBB/44DDS	1.08	2.79	125.3	0.292
3	DBDBBB/33DDS[a]	1.09	7.36	120.4	0.696
4	DBDBBB/44DDS[a]	1.48	6.43	134.6	0.589
5	DBDBBB/33DDS[b]	1.41	21.5	113.3	2.070
6	DBDBBB/44DDS[b]	1.21	15.5	123.1	1.460

[a]Annealing at −30 °C; [b]Annealing at −196 °C; [c]Values at 20 °C; [d]Values at T_g + 30 °C.

Table 4
Mechanical properties involving flexural, impact and hardness parameters.

Entry	Sample	Flexural property[a]			Shore Hardness (HD)
		Stress (MPa)	Modulus (GPa)	Deflection (mm)	
1	DBDBBB/33DDS	80 ± 12	3.030 ± 0.25	4.94 ± 1.14	77.5 ± 0.95
2	DBDBBB/44DDS	57.2 ± 11.2	3.06 ± 0.14	2.86 ± 0.57	59.2 ± 0.5
3	DGEBA/33DDS	142 ± 12.1	3.248 ± 0.88	9.76 ± 2.56	81.2 ± 0.95
4	DGEBA/44DDS	126.3 ± 11.9	2.856 ± 0.24	10.52 ± 1.48	79.7 ± 1.5

[a] Values at breaking point.

acid-treated stainless steel, and thus formed the mechanical connection, such as hook anchor, tenon joint, and riveting before full curing. As to DGEBA/DDS networks, the adhesion strength here reported is about

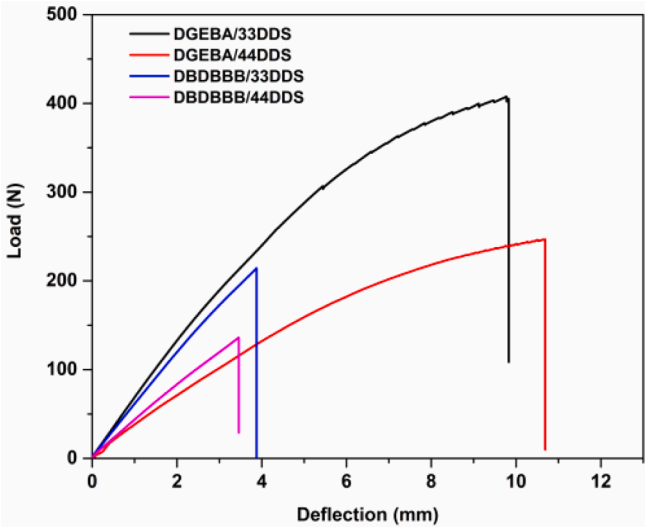

Fig. 6. Representative load–deflection curves of the cured epoxies.

0.80 ~ 1.37 MPa, while DBDBBB/44DDS varied between 2.49 ~ 3.3 MPa [39,40]. Therefore, it suggested that the bio-based DBDBBB/44DDS epoxy possessed a promising market in terms of sustainable adhesive.

3.8. Dielectric properties of epoxy resins

As we know, the low dielectric feature (ε', 2 ~ 5) contributes significantly to the electrical insulators using traditional epoxy resins [41]. Herein, bio-based DBDBBB/DDS was assembled and their dielectric properties were investigated. The dielectric constant (ε') and dielectric loss (ε'')-frequency (f) of the epoxy composites are shown in Fig. 9. The curves indicated that a relatively high ε' value was obtained at low frequency (0.5–5 Hz) in contrast to that at high frequency (Fig. 9a *vs* b). The π-π stacking interaction between aromatic rings was prone to be formed between the symmetric 44DDS in the epoxy resin chains [42]. Thus, more dipolar motifs in the overlapped structure were established. Therefore, the 44DDS-derived networks favored a high dielectric constant in contrast to asymmetric 33DDS analogs. For instance, comparing with DBDBBB/44DDS, the DBDBBB/33DDS gave a low dielectric constant (appropriately 8.5 < 9.75). Moreover, the linear DGEBA is ready for the dielectric constant enhancement. The DGEBA/44DDS displayed the superior ε' over other matrixes, wherein the DGEBA/33DDS and DBDBBB/44DDS roughly represented overlapping curves. On the contrary, the twisted nature of both DBDBBB and 33DDS with low rotational freedom endowed DBDBBB/33DDS with a relatively low dielectric constant. The microstructures for the DBDBBB/33DDS and DBDBBB/44DDS were visible in Fig. 5e and 5f, respectively. Remarkably, the nonlinear chains in the DBDBBB/33DDS blocks might significantly impair both ε' and T_g values [43,44].

Indeed, the dielectric constant (ε') variations are not as spectacular as those of dielectric loss (ε'') *vs* frequency. From the ε''-f plot (Fig. 9c), α, β, and γ relaxations are observed. Firstly, the ε'' peak at about 63 kHz was assigned as β relaxation, commonly assigned to wriggling of hydroxyl formed in the polymerization process. While α relaxation at a frequency of 247 kHz referred to the primary or glass-rubber relaxation, which often originated from the segmental dynamics among the main polymer chains [45]. In addition, the γ-relaxation at high frequency was attributed to the rotation of either methylene or hydroxyether motifs in the polymeric backbone [46]. Apparently, the ε'' varied with frequency. DBDBBB/DDS chains were composed of epoxy resin and the polyolefin motifs in a twisted manner, and thus the networks were in order and did not dramatically change with the increasing frequency. Similar rules remained for partially twisted DGEBA/33DDS. However, for the linear DGEBA/44DDS, the rotation of methylene and hydroxyether motifs in the polymeric backbone was readily aggravated according to the frequency, and resulted in a bigger dielectric loss (Fig. 9c). Accordingly, there is no doubt that the networks herein provided the polymer matrixes with reinforced dielectric constant and loss values (Table S3). For instance, DBDBBB/44DDS respectively showed comparable ε' and ε'' values (9.74, 0.026) to that of poly (vinylidene fluoride) (PVDF) (10 ,0.04) at 1 kHz frequency [47]. Therefore, it is anticipated that such polymeric networks will be a novel substrate for dielectric and energy storage applications, such as high energy density capacitors [48,49].

3.9. Thermal-conductive property

The thermal diffusivity of the system is shown in Fig. 10 and Table S4. It was disclosed that the DGEBA/DDS behaved with higher

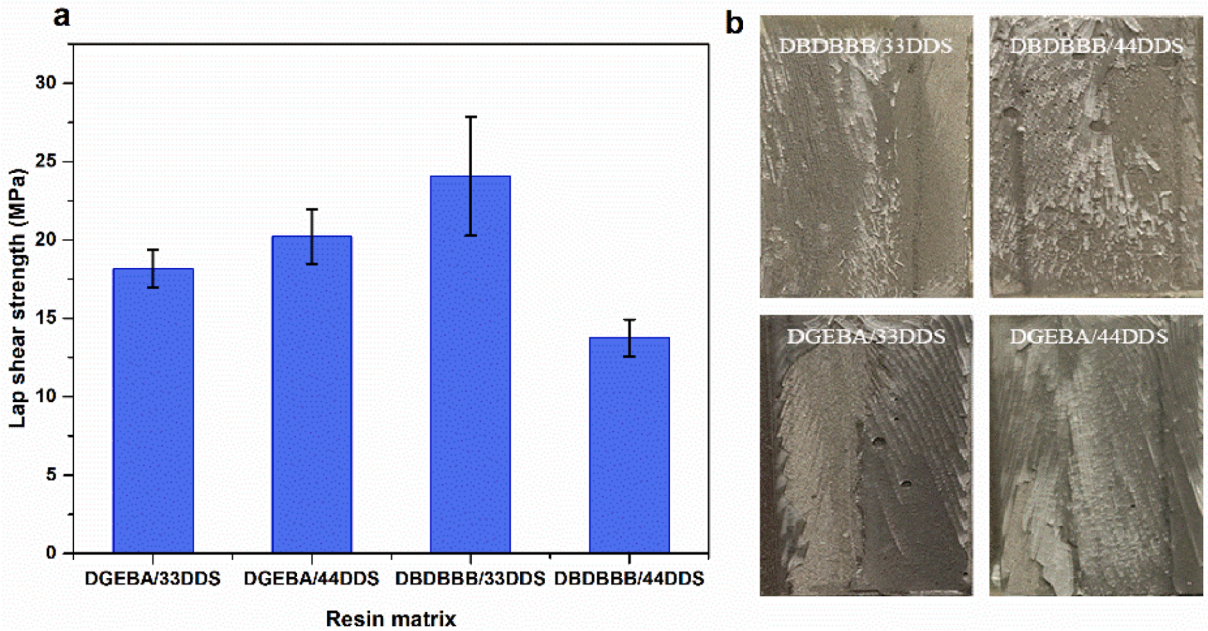

Fig. 7. The lap shear strength distribution (a) and the morphologies of fracture surface (b) of the epoxy resins.

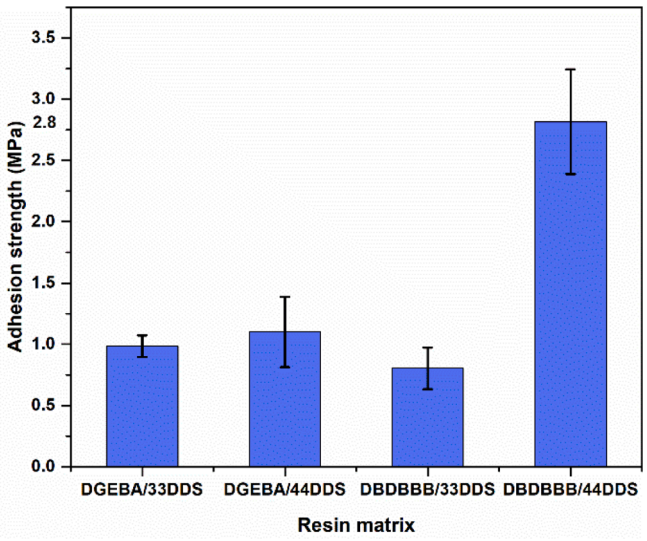

Fig. 8. The adhesion strength of different epoxies.

thermal diffusivities than the DBDBBB/DDS samples. The DGEBA/44DDS had the highest value (about 0.154 mm^2/s), while the others gave close values at about 0.130 mm^2/s. In general, 44DDS endued polymers with higher diffusivity than 33DDS did, meanwhile DGEBA networks exceeded the bio-based DBDBBB.

It is generally acknowledged that the ultralow thermal conductivity (~0.3 W/m•K) of polymers restricts their utilization in electronics, and thus epoxy resin with a higher thermal conductivity is desirable. The DBDBBB/33DDS showed the superiority of thermal conductivity and specific heat (C_p) with the maximums of 0.743 W/m•K, 5.364 J/g•K, respectively (Fig. 10a). Most importantly, the increasing C_p for DBDBBB networks unveiled that the DBDBBB might effectively prevent the heat propagation in the burning process, and thereby increased the fire resistance. Moreover, comparing with the values from previously reported representative works [50], the bio-based DBDBBB/DDS networks furnished relatively high thermal conductivity. In contrast, the epoxy resin from oil-based resources behaved with low to moderate thermal conductivity (<0.5 W/m•K). In particular, the liquid crystal epoxy favored high thermal conductivity due to high-order structures [50,51]. Fig. 10b shows the heating curves of different epoxy networks. Delightedly, the DBDBBB/33DDS favors a dramatically higher heating rate than that of DBDBBB/44DDS. While analogous results for DGEBA analogs. The infrared thermal images in Fig. 10c indicates that DBDBBB/33DDS can heat up to about 100 °C in 15 s, and it confirms that the combination of DBDBBB and 33DDS behaves high thermal conductivity. As it has been presented in Fig. 5e and 5f, for DBDBBB/44DDS, phonon transmission scattering could be too severe due to the distinct gaps or gullies between the dendritic structures [17]. In contrast, as to DBDBBB/33DDS, the compact and interlaced microstructure favored a relative-highly enhanced thermal conductivity. Besides, we can not deny that the aligned networks consisted of polyolefin segments could be responsible for much high thermal conductivity [52,53].

Moreover, the quenching effect on the thermal conductive properties of DBDBBB/DDS samples is also reported (Table S5). After the anneal at −30 °C and −196 °C, the thermal diffusivity and conductivity were effectively enhanced. By this protocol, a high specific heat (C_p) could also reached. Almost certainly, when DBDBBB/44DDS was annealed at −30 °C, the thermal conductivity doubled (0.825 > 0.333 W/m•K) relative to samples quenched at room temperature [54]. To date, in contrast to other net polymers, DBDBBB/33DDS should possess the highest specific heat (C_p) and excellent thermal conductivity [19,55]. The quenching effect provides a facile protocol for the enhancement of the thermal-conductive properties of polymers, and thereby tends to be applied in the exploration of electrical devices and heat-resisting adhesives.

3.10. Burning test

To further explore the flame-retarding properties, the horizontal burning test was carried out. It was disclosed that for DGEBA/DDS, 33DDS- and 44DDS-cured networks dramatically burned with droplet generation, and then extinguished in about 140 s and 155 s. As to DBDBBB, 44DDS greatly enhanced the flame resistance and the flame extinction in 60 s. To our delight, once 33DDS used, DBDBBB/33DDS self-distinguished in 25 s (Fig. 11).

Compared with DGEBA, the DBDBBB system behaved a relatively high decomposition temperature and a significantly increased carbon residue, indicating the fire-resistant nature of bio-based epoxy networks. On the other hand, as mentioned before, the lower thermal diffusivity and higher specific heat values partially took the responsibility for the DBDBBB/DDS flame resistance. Furthermore, a comparison of burning profiles suggested that DBDBBB/33DDS had more compact and continuous structures in the char residue except for some intumescent bubbles on the char surface. In contrast, the char residue for DBDBBB/44DDS exhibited more cracks and failed to isolate heat and gaseous compounds in combustion (Fig. 11d *vs* 11 h). Those concerted elements contributed a lot to enhanced flame retardancy.

As proved by the burning test, the DBDBBB/33DDS behaved flame retardancy. To evaluate the difference, quantitative analysis via micro-scale combustion calorimetry (MCC) was conducted (Fig. 12). The concerning average peak heat release rate (PHRR), total heat release (THR), and the heat release peak temperature for epoxy resins are listed in Table 5. Fig. 12 shows the curves of the heat release rate (HRR) *vs.* temperature at a heating rate of 1 °C/s. The DGEBA/DDS gave higher HRR values than DBDBBB/DDS, about 415 W/g, 260 W/g, respectively (Fig. 12). As to DBDBBB/DDS networks, the THR values for 33DDS are

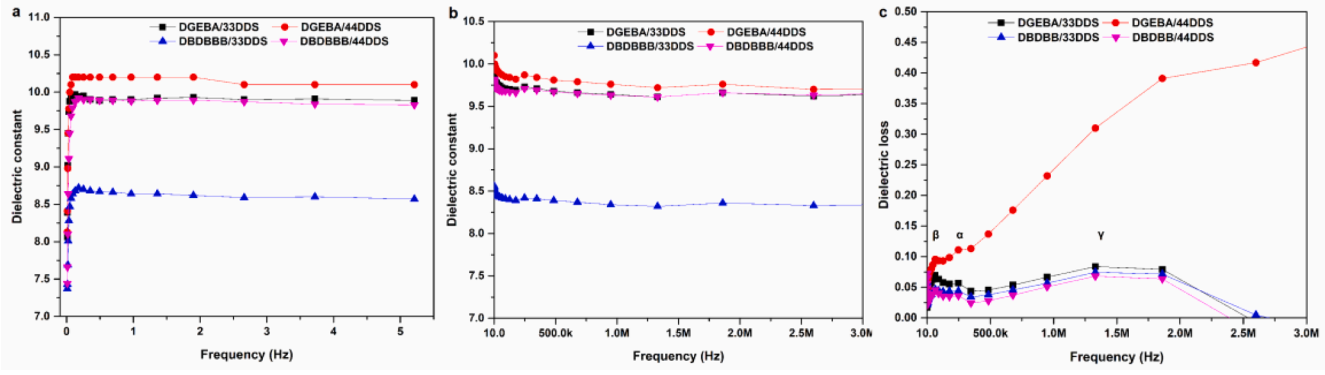

Fig. 9. The dielectric constant *vs* frequency (a, b) and dielectric loss *vs* frequency (c) of the epoxies.

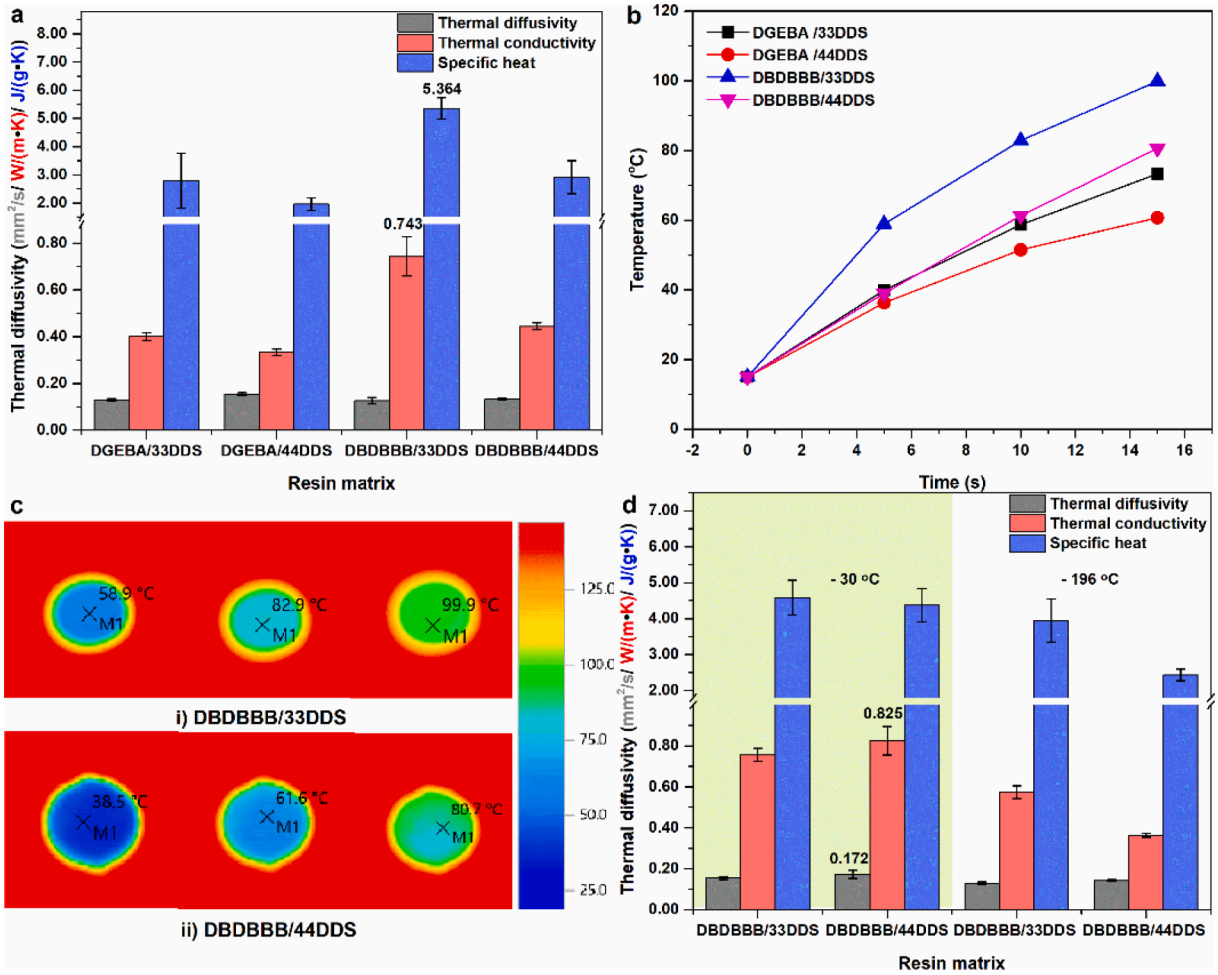

Fig. 10. The thermal conductive properties of the epoxies at room temperature (a) and at low temperatures (d); temperature change curves in the heating process (b); infrared thermal images in the heating process (c).

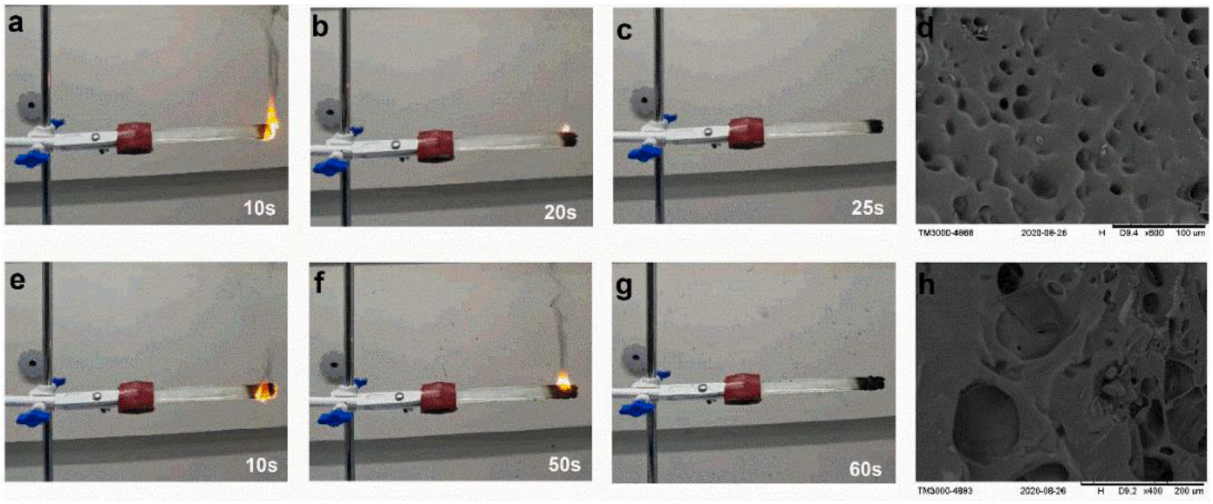

Fig. 11. The burning profile and SEM image of char residue of DBDBBB/33DDS (a-d); DBDBBB/44DDS (e-h).

lower than that of 44DDS-derived polymer (18.98 < 20.93 kJ/g), while the DBDBBB/33DDS favored a higher heat release peak temperature (467.68 > 450.18 °C). Overall, the merits, such as a relatively slow degradation rate and thermally resistant char residue slowed down the pyrolysis reaction in situ endowed the bio-based DBDBBB/33DDS with enhanced flame retardancy.

4. Conclusions

In this text, a new honokiol-based DBDBBB was synthesized and introduced into the novel thermoset epoxy resins. The bio-epoxy resins were fabricated via a solvent-free protocol. The comprehensive investigations of the resultant polymers indicate that the DBDBBB/44DDS

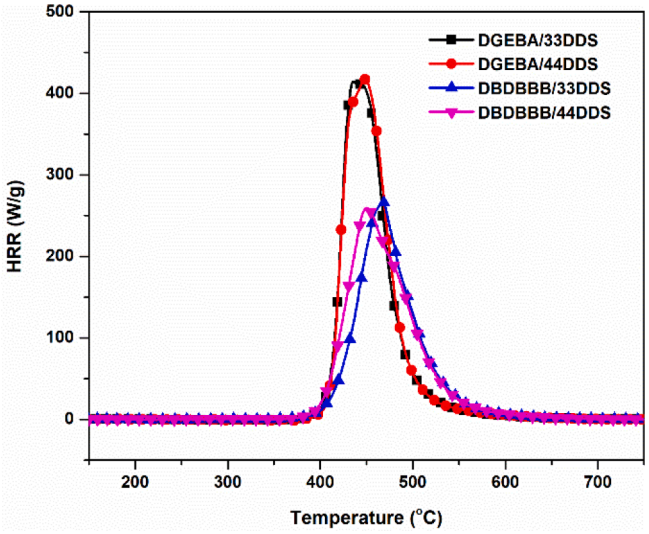

Fig. 12. MCC curves for heat release rate (HRR) versus temperature.

Table 5
Thermal parameters in MCC experiments.

Sample	HRC (J/g•K)	Peak HRR (W/g)	Total HR (kJ/g)	Peak Temp. (°C)
DGEBA/33DDS	421.10	414.47	24.58	435.75
DGEBA/44DDS	418.86	417.14	24.46	448.06
DBDBBB/33DDS	268.93	266.06	18.98	467.68
DBDBBB/44DDS	263.32	259.30	20.93	450.18

has the highest T_{d5} value among bio-based epoxy resins. Its pyrolysis temperature reached about 398 °C, and surpassed that of DGEBA counterparts even proceeding in air. Due to the stably twisted epoxy resin and polyolefin motifs, DBDBBB/44DDS yielded an advantageous dielectric constant and loss value (9.74, 0.026) at 1 kHz frequency. The ordered and interlaced microstructure of DBDBBB/33DDS favored relative-highly enhanced thermal conductive properties with excellent thermal conductivity and specific heat (C_p) up to 0.743 W/m•K, 5.364 J/g•K, respectively. Moreover, MCC and burning test suggested enhanced fire resistance for DBDBBB/33DDS as well. Besides, for bio-based DBDBBB/DDS, the mechanic properties including lap shear strength and impact strength as well as adhesion test have proved to be good even much better than DGEBA/DDS.

Declaration of Competing Interest

The authors declare that they have no known competing financial interests or personal relationships that could have appeared to influence the work reported in this paper.

Acknowledgments

This work was supported by the National Natural Science Foundation of China (Grant No. 21908107) and the Jiangsu Synergetic Innovation Center for Advanced Bio-Manufacture (grants XTE1827).

Appendix A. Supplementary data

Supplementary data to this article can be found online at https://doi.org/10.1016/j.cej.2021.128647.

References

[1] M. Decostanzi, R. Auvergne, B. Boutevin, S. Caillol, Biobased phenol and furan derivative coupling for the synthesis of functional monomers, Green Chem. 21 (4) (2019) 724–747, https://doi.org/10.1039/C8GC03541E.
[2] V. Froidevaux, C. Negrell, S. Caillol, J.P. Pascault, B. Boutevin, Biobased amines: from synthesis to polymers; present and future, Chem. Rev. 116 (2016) 14181–14224.
[3] R. Saidur, E.A. Abdelaziz, A. Demirbas, M.S. Hossain, S. Mekhilef, A review on biomass as a fuel for boilers, Renew. Sustain. Energy Rev. 15 (5) (2011) 2262–2289, https://doi.org/10.1016/j.rser.2011.02.015.
[4] R.M. O'Dea, J.A. Willie, T.H. Epps, 100th anniversary of macromolecular science viewpoint: polymers from lignocellulosic biomass. Current challenges and future opportunities, ACS Macro Lett. 9 (2020) 476–493.
[5] M.Z. Oulame, F. Pion, S. Allauddin, K.V.S.N. Raju, P.-H. Ducrot, F. Allais, Renewable alternating aliphatic-aromatic poly(ester-urethane)s prepared from ferulic acid and bio-based diols, Eur. Polym. J. 63 (2015) 186–193, https://doi.org/10.1016/j.eurpolymj.2014.11.031.
[6] I. Lee Hia, E.-S. Chan, S.-P. Chai, P. Pasbakhsh, A novel repeated self-healing epoxy composite with alginate multicore microcapsules, J. Mater. Chem. A 6 (18) (2018) 8470–8478, https://doi.org/10.1039/C8TA01783B.
[7] M.V. Maffini, B.S. Rubin, C. Sonnenschein, A.M. Soto, Endocrine disruptors and reproductive health: the case of bisphenol-A, Mol. Cell. Endocrinol. 254-255 (2006) 179–186, https://doi.org/10.1016/j.mce:2006.04.033.
[8] Y. Tian, Q. Wang, L. Shen, Z. Cui, L. Kou, J. Cheng, J. Zhang, A renewable resveratrol-based epoxy resin with high Tg, excellent mechanical properties and low flammability, Chem. Eng. J. 383 (2020), 123124.
[9] Y. Qi, Z. Weng, K. Zhang, J. Wang, S. Zhang, C. Liu, X. Jian, Magnolol-based bio-epoxy resin with acceptable glass transition temperature, processability and flame retardancy, Chem. Eng. J. 387 (2020), 124115.
[10] J. Dai, Y. Peng, N.a. Teng, Y. Liu, C. Liu, X. Shen, S. Mahmud, J. Zhu, X. Liu, High-performing and fire-resistant biobased epoxy resin from renewable sources, ACS Sustainable Chem. Eng. 6 (6) (2018) 7589–7599, https://doi.org/10.1021/acssuschemeng.8b00439.
[11] C. Li, H. Fan, T. Aziz, C. Bittencourt, L. Wu, D. Wang, P. Dubois, Biobased epoxy resin with low electrical permissivity and flame retardancy: from environmental friendly high-throughput synthesis to properties, ACS Sustainable Chem. Eng. 6 (2018) 8856–8867.
[12] J. Miao, L. Yuan, G. Liang, A. Gu, Biobased bismaleimide resins with high renewable carbon content, heat resistance and flame retardancy via a multi-functional phosphate from clove oil, Mater. Chem. Front. 3 (2019) 78–85.
[13] S.L. Kristufek, G. Yang, L.A. Link, B.J. Rohde, M.L. Robertson, K.L. Wooley, Synthesis, characterization, and cross-linking strategy of a quercetin-based epoxidized monomer as a naturally-derived replacement for BPA in epoxy resins, ChemSusChem 9 (16) (2016) 2135–2142, https://doi.org/10.1002/cssc.201600392.
[14] W. Xie, S. Huang, D. Tang, S. Liu, J. Zhao, Biomass-derived Schiff base compound enabled fire-safe epoxy thermoset with excellent mechanical properties and high glass transition temperature, Chem. Eng. J. 394 (2020), 123667.
[15] S. Chen, Z. Xu, D. Zhang, Synthesis and application of epoxy-ended hyperbranched polymers, Chem. Eng. J. 343 (2018) 283–302, https://doi.org/10.1016/j.cej.2018.03.014.
[16] H. Mei, J. Xia, D. Han, S. Xiao, J. Deng, L. Cheng, Dramatic increase in electrical conductivity in epoxy composites with uni-directionally oriented laminae of carbon nanotubes, Chem. Eng. J. 304 (2016) 970–976, https://doi.org/10.1016/j.cej.2016.07.025.
[17] Y. Guo, K. Ruan, X. Shi, X. Yang, J. Gu, Factors affecting thermal conductivities of the polymers and polymer composites: a review, Compos. Sci. Technol. 193 (2020) 108134, https://doi.org/10.1016/j.compscitech.2020.108134.
[18] S. Li, X. Yu, H. Bao, N. Yang, High thermal conductivity of bulk epoxy resin by bottom-up parallel-linking and strain: a molecular dynamics study, J. Phys. Chem. C 122 (2018) 13140–13147.
[19] Y.-X. Fu, Z.-X. He, D.-C. Mo, S.-S. Lu, Thermal conductivity enhancement with different fillers for epoxy resin adhesives, Appl. Therm. Eng. 66 (1-2) (2014) 493–498, https://doi.org/10.1016/j.applthermaleng.2014.02.044.
[20] Y. Sun, B.o. Tang, W. Huang, S. Wang, Z. Wang, X. Wang, Y. Zhu, C. Tao, Preparation of graphene modified epoxy resin with high thermal conductivity by optimizing the morphology of filler, Appl. Therm. Eng. 103 (2016) 892–900, https://doi.org/10.1016/j.applthermaleng.2016.05.005.
[21] Z. Qu, K. Wu, W. Meng, B. Nan, Z. Hu, C.A. Xu, Z. Tan, Q. Zhang, H. Meng, J. Shi, Surface coordination of black phosphorene for excellent stability, flame retardancy and thermal conductivity in epoxy resin, Chem. Eng. J. 397 (2020), 125416.
[22] Z. Qu, K. Wu, E. Jiao, W. Chen, Z. Hu, C. Xu, J. Shi, S. Wang, Z. Tan, Surface functionalization of few-layer black phosphorene and its flame retardancy in epoxy resin, Chem. Eng. J. 382 (2020), 122991.
[23] X.-H. Shi, Y.-J. Xu, J.-W. Long, Q. Zhao, X.-M. Ding, L.i. Chen, Y.-Z. Wang, Layer-by-layer assembled flame-retardant architecture toward high-performance carbon fiber composite, Chem. Eng. J. 353 (2018) 550–558, https://doi.org/10.1016/j.cej.2018.07.146.
[24] M. Cui, L. Zhang, P. Lou, X. Zhang, X. Han, Z. Zhang, S. Zhu, Study on thermal degradation mechanism of heat-resistant epoxy resin modified with carboranes, Polym. Degrad. Stab. 176 (2020), 109143.
[25] H. Duan, Y. Chen, S. Ji, R. Hu, H. Ma, A novel phosphorus/nitrogen-containing polycarboxylic acid endowing epoxy resin with excellent flame retardance and mechanical properties, Chem. Eng. J. 375 (2019), 121916.

[26] C. Nyambo, C.A. Wilkie, Layered double hydroxides intercalated with borate anions: Fire and thermal properties in ethylene vinyl acetate copolymer, Polym. Degrad. Stab. 94 (2009) 506–512.
[27] Q. Wang, J.P. Undrell, Y. Gao, G. Cai, J.-C. Buffet, C.A. Wilkie, D. O'Hare, Synthesis of flame-retardant polypropylene/LDH-borate nanocomposites, Macromolecules 46 (15) (2013) 6145–6150, https://doi.org/10.1021/ma401133s.
[28] H. Gu, J. Guo, Q. He, S. Tadakamalla, X.i. Zhang, X. Yan, Y. Huang, H.A. Colorado, S. Wei, Z. Guo, Flame-retardant epoxy resin nanocomposites reinforced with polyaniline-stabilized silica nanoparticles, Ind. Eng. Chem. Res. 52 (23) (2013) 7718–7728, https://doi.org/10.1021/ie400275n.
[29] Y. Qiu, L. Qian, H. Feng, S. Jin, J. Hao, Toughening effect and flame-retardant behaviors of phosphaphenanthrene/phenylsiloxane bigroup macromolecules in epoxy thermoset, Macromolecules 51 (23) (2018) 9992–10002, https://doi.org/10.1021/acs.macromol.8b02090.s001.
[30] X. Wang, E.N. Kalali, D.-Y. Wang, Renewable cardanol-based surfactant modified layered double hydroxide as a flame retardant for epoxy resin, ACS Sustainable Chem. Eng. 3 (12) (2015) 3281–3290, https://doi.org/10.1021/acssuschemeng.5b00871.
[31] M. Zhi, Q. Liu, H. Chen, X. Chen, S. Feng, Y. He, Thermal stability and flame retardancy properties of epoxy resin modified with functionalized graphene oxide containing phosphorus and silicon elements, ACS Omega 4 (6) (2019) 10975–10984, https://doi.org/10.1021/acsomega.9b00852.
[32] J. Meng, Y. Zeng, G. Zhu, J. Zhang, P. Chen, Y. Cheng, Z. Fang, K. Guo, Sustainable bio-based furan epoxy resin with flame retardancy, Polym. Chem. 10 (19) (2019) 2370–2375, https://doi.org/10.1039/C9PY00202B.
[33] J. Zhao, J. Zhang, L. Wang, J. Li, T. Feng, J. Fan, L. Chen, J. Gu, Superior wave-absorbing performances of silicone rubber composites via introducing covalently bonded SnO_2@MWCNT absorbent with encapsulation structure, Compos. Commun. 22 (2020), 100486.
[34] N. Teng, S. Yang, J. Dai, S. Wang, J. Zhao, J. Zhu, X. Liu, Making benzoxazine greener and stronger: renewable resource, microwave irradiation, green solvent, and excellent thermal properties, ACS Sustainable Chem. Eng. 7 (2019) 8715–8723.
[35] M.K. Hassan, S.J. Tucker, A. Abukmail, J.S. Wiggins, K.A. Mauritz, Polymer chain dynamics in epoxy based composites as investigated by broadband dielectric spectroscopy, Arabian J. Chem. 9 (2) (2016) 305–315, https://doi.org/10.1016/j.arabjc.2015.07.016.
[36] A.L. Cholli, J.J. Dumais, A.K. Engel, L.W. Jelinski, Aromatic ring flips in a semicrystalline polymer, Macromolecules 17 (11) (1984) 2399–2404, https://doi.org/10.1021/ma00141a032.
[37] M. Aliakbari, O.M. Jazani, M. Sohrabian, Epoxy adhesives toughened with waste tire powder, nanoclay, and phenolic resin for metal-polymer lap-joint applications, Prog. Org. Coat. 136 (2019), 105291.
[38] V. Pang, Z.J. Thompson, G.D. Joly, F.S. Bates, L.F. Francis, Adhesion strength of block copolymer toughened epoxy on aluminum, ACS Appl. Polym. Mater. 2 (2) (2020) 464–474, https://doi.org/10.1021/acsapm.9b00909.s001.
[39] S. Ma, X. Liu, Y. Jiang, Z. Tang, C. Zhang, J. Zhu, Bio-based epoxy resin from itaconic acid and its thermosets cured with anhydride and comonomers, Green Chem. 15 (1) (2013) 245–254, https://doi.org/10.1039/C2GC36715G.
[40] T. Okamatsu, Effect on the toughness and adhesion properties of epoxy resin modified with silyl-crosslinked urethane microsphere, Polymer 43 (3) (2002) 721–730, https://doi.org/10.1016/S0032-3861(01)00645-0.
[41] J. Wei, L. Zhu, Intrinsic polymer dielectrics for high energy density and low loss electric energy storage, Prog. Polym. Sci. 106 (2020), 101254.
[42] A.S. Shetty, J. Zhang, J.S. Moore, Aromatic π-stacking in solution as revealed through the aggregation of phenylacetylene macrocycles, J. Am. Chem. Soc. 118 (5) (1996) 1019–1027, https://doi.org/10.1021/ja9528893.
[43] W. Peng, X. Huang, J. Yu, P. Jiang, W. Liu, Electrical and thermophysical properties of epoxy/aluminum nitride nanocomposites: effects of nanoparticle surface modification, Compos. A Appl. Sci. Manuf. 41 (9) (2010) 1201–1209, https://doi.org/10.1016/j.compositesa:2010.05.002.
[44] L. Gao, Q. Zhang, H. Li, S. Yu, W. Zhong, G. Sui, X. Yang, Effect of epoxy monomer structure on the curing process and thermo-mechanical characteristics of tri-functional epoxy/amine systems: a methodology combining atomistic molecular simulation with experimental analyses, Polym. Chem. 8 (2017) 2016–2027.
[45] E. Serrano, G. Kortaberria, P. Arruti, A. Tercjak, I. Mondragon, Molecular dynamics of an epoxy resin modified with an epoxidized poly(styrene–butadiene) linear block copolymer during cure and microphase separation processes, Eur. Polym. J. 45 (4) (2009) 1046–1057, https://doi.org/10.1016/j.eurpolymj.2008.12.018.
[46] M. Beiner, K.L. Ngai, Interrelation between primary and secondary relaxations in polymerizing systems based on epoxy resins, Macromolecules 38 (16) (2005) 7033–7042, https://doi.org/10.1021/ma050384j.
[47] J. Lao, H. Xie, Z. Shi, G. Li, B. Li, G.-H. Hu, Q. Yang, C. Xiong, Flexible regenerated cellulose/boron nitride nanosheet high-temperature dielectric nanocomposite films with high energy density and breakdown strength, ACS Sustainable Chem. Eng. 6 (5) (2018) 7151–7158, https://doi.org/10.1021/acssuschemeng.8b01219.s001.
[48] Prateek, V.K. Thakur, R.K. Gupta, Recent progress on ferroelectric polymer-based nanocomposites for high energy density capacitors: synthesis, dielectric properties, and future aspects, Chem. Rev. 116 (2016) 4260–4317.
[49] S. Chen, G. Meng, B. Kong, B. Xiao, Z. Wang, Z. Jing, Y. Gao, G. Wu, H. Wang, Y. Cheng, Asymmetric alicyclic amine-polyether amine molecular chain structure for improved energy storage density of high-temperature crosslinked polymer capacitor, Chem. Eng. J. 387 (2020), 123662.
[50] X. Yang, J. Zhu, D. Yang, J. Zhang, Y. Guo, X. Zhong, J. Kong, J. Gu, High-efficiency improvement of thermal conductivities for epoxy composites from synthesized liquid crystal epoxy followed by doping BN fillers, Compos. Part B Eng. 185 (2020), 107784.
[51] M. Akatsuka, Y. Takezawa, Study of high thermal conductive epoxy resins containing controlled high-order structures, J. Appl. Polym. Sci. 89 (9) (2003) 2464–2467, https://doi.org/10.1002/app.12489.
[52] Y. Xu, D. Kraemer, B. Song, Z. Jiang, J. Zhou, J. Loomis, J. Wang, M. Li, H. Ghasemi, X. Huang, X. Li, G. Chen, Nanostructured polymer films with metal-like thermal conductivity, Nat. Commun. 10 (2019) 1771.
[53] V. Singh, T.L. Bougher, A. Weathers, Y.e. Cai, K. Bi, M.T. Pettes, S.A. McMenamin, W. Lv, D.P. Resler, T.R. Gattuso, D.H. Altman, K.H. Sandhage, L.i. Shi, A. Henry, B. A. Cola, High thermal conductivity of chain-oriented amorphous polythiophene, Nat. Nanotech. 9 (5) (2014) 384–390, https://doi.org/10.1038/nnano.2014.44.
[54] M. Harada, M. Ochi, M. Tobita, T. Kimura, T. Ishigaki, N. Shimoyama, H. Aoki, Thermal-conductivity properties of liquid-crystalline epoxy resin cured under a magnetic field, J. Polym. Sci. B Polym. Phys. 41 (14) (2003) 1739–1743, https://doi.org/10.1002/polb.10531.
[55] C. Huang, X. Qian, R. Yang, Thermal conductivity of polymers and polymer nanocomposites, Mater. Sci. Eng.: R: Rep. 132 (2018) 1–22.